Salt-inducible kinase inhibition promotes the adipocyte thermogenic program and adipose tissue browning

Fubiao Shi[1]*, Flaviane de Fatima Silva[1,2], Dianxin Liu[1], Clara Türk[4], Marcus Krüger[4,5], Sheila Collins[1,3]*

[1]Division of Cardiovascular Medicine, Department of Medicine, Vanderbilt University Medical Center, Nashville, TN 37232, USA

[2]Department of Physiology and Biophysics, Institute of Biomedical Sciences, University of Sao Paulo, Sao Paulo 05508-000, Brazil

[3]Department of Molecular Physiology and Biophysics, Vanderbilt University School of Medicine, Nashville, TN 37232, USA

[4]CECAD Research Center, Institute for Genetics, University of Cologne, Cologne 50931 Germany

[5]Center for Molecular Medicine (CMMC), University of Cologne, Cologne 50931, Germany

*Corresponding authors.

Correspondence Address:

Sheila Collins, Ph.D.

Vanderbilt University Medical Center
342B Preston Research Building
2220 Pierce Avenue, Nashville, TN 37232
Email: sheila.collins@vumc.org

Fubiao Shi, Ph.D.

Vanderbilt University Medical Center
340 Preston Research Building
2220 Pierce Avenue, Nashville, TN 37232
Email: fubiao.shi@vumc.org

Abstract

Norepinephrine stimulates the adipose tissue thermogenic program through a β-adrenergic receptor (βAR) - cyclic adenosine monophosphate (cAMP) - protein kinase A (PKA) signaling cascade. Previous work from our lab showed that noncanonical activation of the mechanistic target of rapamycin complex 1 (mTORC1) by PKA is required for the βAR-stimulation of adipose tissue browning. However, the downstream events triggered by mTORC1 activation that drive this thermogenic response are not well understood. In this study, we used a proteomic approach of Stable Isotope Labeling by/with Amino acids in Cell culture (SILAC) to characterize the global protein phosphorylation profile in brown adipocytes with β-agonist isoproterenol stimulation and identified salt-inducible kinase 3 (SIK3) as a candidate mTORC1 substrate. SIK3 interacts with RAPTOR, the defining component of the mTORC1 complex, and is phosphorylated at Ser^{884} in a mTORC1-dependent manner. Pharmacological SIK inhibition by a pan-SIK inhibitor (HG-9-91-01) in brown adipocytes increases basal *Ucp1* gene expression and restores its expression upon either mTORC1 or PKA blockades. Short-hairpin RNA knockdown of *Sik3* augments, while overexpression of SIK3 suppresses, *Ucp1* gene expression in brown adipocytes. In addition, CRISPR gene-edited *Sik3*-/- brown adipocytes show enhanced *Ucp1* gene expression at basal conditions and after Iso stimulation. Finally, a SIK inhibitor well-tolerated *in* vivo (YKL-05-099) can stimulate adipose tissue browning and thermogenic gene expression in mouse subcutaneous inguinal adipose tissue, supporting an essential role of SIK inhibition in regulating the adipose tissue browning program *in vivo*. Taken together, our data reveal that salt-inducible kinases function as a phosphorylation switch for β-adrenergic activation to drive the adipose thermogenic program and suggest that maneuvers targeting SIKs could be beneficial for obesity and related metabolic disease.

Introduction

Obesity is a major risk factor for diabetes, cardiovascular disease, and certain types of cancer [1]. The global epidemic of obesity has been a heavy burden to the public health and represents an unmet medical need that requires more effort in both basic and translational research. Adipose tissue, as an endocrine organ, plays an essential role in the pathophysiology of obesity. The white adipose tissue (WAT) functions as a sink to preserve excessive calories in the form of lipids, while the brown adipose tissue (BAT) can actively consume glucose and fatty acids and dissipate them as heat through a futile metabolic process via the mitochondrial uncoupling protein 1 (UCP1).

In rodents, brown-like UCP1-positive (beige) adipocytes can be induced in subcutaneous inguinal WAT (iWAT) after cold exposure, or treatment with selective agonists for β_3-adrenergic receptor (β_3AR) and peroxisome proliferator-activated receptor gamma (PPARγ) - a process termed adipose tissue beiging or browning [2-7]. In adult humans, functional BAT has been identified by using the ^{18}F-deoxyglucose (FDG)-positron emission tomography (PET) imaging method in healthy individuals after cold exposure but not in subjects acclimated to a thermoneutral temperature [8-10]. These studies, together with others, have spurred recent efforts to explore the potential of BAT as a therapeutic target for obesity-related metabolic disease [11]. BAT plays a crucial role in systematic metabolic homeostasis, blood glucose and lipid control. In both rodents and humans, the amount of active BAT is highly correlated with resistance to weight gain and improvement in insulin sensitivity [9; 12]. Individuals with detectable BAT correlated with a lower prevalence of cardiometabolic diseases, suggesting that BAT might play a role in mitigating the deleterious effects of obesity while also promoting cardiometabolic health [13].

Better understanding of the mechanisms of BAT activation by βAR agonists could provide new insights for the discovery of novel targets to intervene in obesity and cardiometabolic disease. As a potent thermogenic stimulator of BAT, cold temperature increases the sympathetic nervous system (SNS) to release norepinephrine, which activates the βAR-cAMP-PKA signaling cascade to drive the expression of a panel of thermogenic and mitochondrial biogenesis genes, including UCP1 and Peroxisome proliferator-activated receptor Gamma (PPARγ) Coactivator-1α (PGC1α) (reviewed in [14; 15]).

As a central regulator of the brown fat thermogenic program, PGC1α can directly regulate *Ucp1* expression (in cooperation with PPARγ) and promote mitochondrial biogenesis [16]. Several

mechanisms of reversible acetylation have been reported to modulate PGC1α activity [17]. For example, histone acetyltransferase GCN5 acetylates PGC1α in the internal region of the protein and serves to repress its activity [18]. This internal acetylation could be removed by the deacetylase SIRT1 [19]. A recent study showed that N-α-acetyltransferase 10 protein (NAA10) catalyzes the N-terminal acetylation of PGC1α and inhibits PGC1α activity by preventing its recruitment to the *Ucp1* promoter [20]. However it is not yet known whether N-α-acetylation of PGC1α is reversible and how it is regulated [21].

Early work from our lab showed that p38 mitogen-activated protein kinase is an important component of the PKA-stimulated signaling cascade for *Ucp1* and *Pgc1α* gene expression in brown adipocytes [22-24]. More recently, we have made the novel observation that activation of the mechanistic target of rapamycin complex 1 (mTORC1) by PKA is also essential for β-adrenergic stimulation of adipose tissue browning [25]. Pharmacological mTOR inhibition by rapamycin blunts adipose tissue browning in response to the β_3AR-selective agonist CL-316,243 (CL) treatment [25], and adipose-specific deletion of Raptor, the defining component of mTORC1, impairs brown/beige adipocyte expansion during cold challenge [25]. Unlike the well-established insulin signaling pathway that activates mTORC1 through the action of Protein Kinase B (AKT), the activation of mTORC1 by βAR signaling depends on the PKA phosphorylation of Ser^{791} in RAPTOR and three sites in mTOR [25]. Consistent with our study, several other groups also have demonstrated the essential role of mTORC1 in the regulation of brown adipose tissue function [26-28]. In addition, mTORC1 activation has also been identified to underpin the thermogenic effect in other signaling pathways and physiological contexts, such as natriuretic peptide/cGMP signaling [29] and asparagine feeding [30].

Salt-inducible kinases are a subgroup of the AMP-activated protein kinase (AMPK) family. The three SIK isoforms, SIK1, SIK2, and SIK3 are widely expressed and have been shown to be important regulators of hormonal signaling and metabolism in several tissues [31; 32]. Activation of SIKs depends on their phosphorylation in the activation domain by the upstream kinase liver kinase B1 (LKB1). Several PKA phosphorylation sites have been identified in SIKs, and their phosphorylation facilitates the interaction of SIKs with 14-3-3 proteins and results in SIK inhibition [33]. Several SIK substrates have been identified, including class IIa histone deacetylases (HDACs) and cAMP-regulated transcriptional coactivators (CRTCs) [31; 32]. When activated, SIKs phosphorylate HDACs and CRTCs and prevent their nuclear translocation. On

the other hand, when SIK activity is inhibited by PKA phosphorylation, HDACs and CRTCs are dephosphorylated and can translocate to the nucleus to regulate the expression of their target genes.

All three SIK isoforms are expressed in rodent and human adipocytes and adipose tissues, with the expression of SIK2 being most abundant [34; 35]. In this regard, SIK2 has been linked to the regulation of insulin signaling, adipogenesis and lipogenesis in adipocytes [36-39]. In adipose tissue from obese or insulin-resistant individuals, SIK2 and SIK3 mRNAs are down-regulated [35], but the functional consequences of this are still unclear. In mouse models, expression of the thermogenic gene *Ucp1* is increased in subcutaneous iWAT of *Sik1/2* double knockout mice, but in neither *Sik1* or *Sik2* single knockout mice [34], suggesting a functional redundancy between SIK isoforms, at least when one or the other is constitutively absent. At thermoneutrality, but not room temperature, global deletion of *Sik2* increases *Ucp1* expression and the response to β-agonist treatment [40]. Together these studies indicate that SIKs may have redundant but also unique roles in the control of adipose tissue metabolism and that there is still much to be understood about their role in this tissue. Although disturbed glucose and lipid metabolism was observed in *Sik3* global knockout mice [41], the role of SIK3 in the control of adipose tissue metabolism, especially of the thermogenic program, is not known. Interestingly, adipose tissue specific ablation of LKB1, the upstream kinase for SIK activation, promotes BAT expansion and WAT browning [34; 42]. In the absence of LKB1 SIKs cannot be activated, and thus their substrates CRTC3 and HDAC4 that can now be localized in the nucleus, are likely involved in these browning phenotypes [34; 42].

In this study, we hypothesized that the different metabolic effects of insulin and norepinephrine in brown adipocytes are mediated through distinct mTORC1 substrates. To elucidate downstream mechanisms of PKA-dependent mTORC1 activation, we employed a phosphoproteomics approach to profile phosphoproteins in response to βAR signaling in brown adipocytes and identified salt-inducible kinase 3 (SIK3) as a candidate mTORC1 substrate. SIK3 interacts with RAPTOR and is phosphorylated in a mTORC1-dependent manner. Our results also show that in brown adipocytes *in vitro* SIK inhibition or targeted SIK3 deletion increases, while its over-expression suppresses, expression of key thermogenic genes. Furthermore, pharmacological SIK inhibition *in vivo* promotes thermogenic gene expression and adipose tissue browning. Our study defines an essential role of SIK3 in the regulation of brown adipocyte thermogenic gene program and suggested pharmacological SIK inhibition is a potential intervention for obesity and metabolic disease.

Results

Phosphoproteomic study identifies SIK3 as a mTORC1 substrate in murine brown adipocytes

We employed a proteomic approach of Stable Isotope Labeling by/with Amino acids in Cell culture (SILAC) to compare the global protein phosphorylation profile in brown adipose tissue (BAT) adipocytes after either β-agonist isoproterenol (Iso) or insulin (Ins) stimulation, in combination with or without the mTORC1 inhibitor rapamycin (Rapa) (**Figure 1A**). As a well-established substrate of the mTOR signaling pathway, phosphorylation of Ser^{240} in ribosomal protein S6 was increased both by Iso and Ins and blocked by rapamycin, while phosphorylation of Ser^{473} in AKT was increased only by Ins and unaffected by Iso or Rapa, as its activation is upstream of mTORC1 (**Figure 1B and 1C**). These results mirror our previous findings [25]. Interestingly, among several other proteins, the phosphorylation of SIK3 on Ser^{884} (S^{884}) was increased by Iso, blocked by Rapa, but unaffected by Ins (**Figure 1B and 1C**), suggesting a mTOR-dependent effect. The S^{884} site conforms to identified mTOR phosphorylation sites [43] and is found in the C-terminal regulatory domains of SIK3 but not in the other two salt-inducible kinases SIK1 or SIK2 (**Figure 1D**). Subsequent experiments showed that SIK3 can be immunoprecipitated with RAPTOR, the defining component of mTORC1 and which is known to present substrates to the mTOR kinase [44; 45], indicating the physical interaction of SIK3 with mTORC1 (**Figure 1E**).

SIK inhibition stimulates *Ucp1* gene expression in HIB-1B brown adipocytes

To understand the role of SIK3 in regulating the brown adipocyte thermogenic gene program, we first examined the effect of pharmacological SIK inhibition in HIB-1B murine brown adipocytes. Several compounds have been reported to inhibit SIK activities, including the pan-SIK inhibitors HG-9-91-01 (HG) [46; 47], YKL-05-099 (YKL) [48] and the SIK3-selective inhibitor pterosin B (PTB) [49; 50]. Our results showed that all three compounds increase basal expression of the *Ucp1* gene in HIB-1B cells in a dose-dependent manner (**Figure 2A-2C**). While the βAR agonist isoproterenol (Iso) is a more potent stimulator, the point here is that even in the absence of Iso there is nevertheless an increase in basal *Ucp1* expression in basal conditions in which βAR activity is low.

Because inhibition of PKA or mTORC1 prevents β-agonist stimulated *Ucp1* expression and adipose browning [25], we next asked whether SIK inhibition could override the effects of PKA

or mTORC1 inhibitors. Pretreatment with HG increased *Ucp1* expression under basal unstimulated conditions and potentiated the response to Iso. HG also restored *Ucp1* expression after either PKA inhibition by H89 (**Figure 2D**) or mTORC1 inhibition by Rapa (**Figure 2E**). This would place SIK inhibition as a step downstream of the PKA-mTORC1 signaling cascades after β-adrenergic stimulation.

Since this effect of SIK inhibition on *Ucp1* gene expression is not SIK isoform-specific, we next sought to dissect the role of SIK3 by specific manipulation of SIK3 gene expression in HIB-1B cells. Short hairpin RNA (shRNA) knockdown of *Sik3* increased *Ucp1* gene expression in HIB-1B cells after Iso stimulation (**Figure 2F**). In addition, over-expression of SIK3 protein in HIB-1B cells suppressed *Ucp1* expression (**Figure 2G**), further supporting the notion that SIK3 functions as a suppressor of brown adipocyte thermogenic gene program.

SIK3 deletion in brown adipocytes increases thermogenic gene expression

We next utilized CRIPSR/Cas9 gene editing to specifically knockout the *Sik3* gene in HIB-1B brown adipocytes using a previously established guide RNA (gRNA) expression construct [51]. Sequencing results showed that three major mutations were generated in the *Sik3* gene: a single-nucleotide deletion (ΔT), a two-nucleotide deletion (ΔTC) and a single-nucleotide insertion (iT) (**Figure 3A**). Each of these mutations will generate transcripts with frameshifts from the Ala^{165} (A^{165}) residue, resulting in truncated proteins due to premature stop codon (**Figure 3A**). Two gene-edited clones, SC19 and SC13, were identified to bear two frame-shift mutations and considered *Sik3*-/- brown adipocytes (**Figure 3A**). Western blot analysis showed that SIK3 protein was completely absent in these *Sik3*-/- adipocyte clones but not in the non-targeting control (NTC) cells (**Figure 3B**). Interesting, the expression of PGC1α and certain mitochondrial oxidative phosphorylation (OXPHOS) proteins are increased in *Sik3*-/- adipocytes (**Figure 3B**). In addition, quantitative PCR (QPCR) analysis showed that *Sik3* mRNA was significantly reduced in the SC19 and SC13 brown adipocytes (**Figure 3C**), potentially due to nonsense-mediated mRNA decay [52]. Expression of *Ucp1* and *Pgc1α* mRNA were increased in *Sik3*-deficient brown adipocytes both at basal conditions and after Iso stimulation (**Figure 3C**). This data is consistent with the *Sik3* knockdown and over-expression experiments (**Figure 2E - 2F**). Of note, although the SIK3 protein was absent from both SC19 and SC13 clones, the increases in *Ucp1* and *Pgc1α* mRNA expression

were more robust in clone SC13 (**Figure 3C**), possibly due to clonal variations or other potential off-target effects [53].

Phosphorylation of SIK3 by PKA is essential for inhibition to drive thermogenic gene expression

With the generation of *Sik3*-/- HIB-1B brown adipocytes, we next established a SIK3 re-expression procedure to evaluate the functional domains of the SIK3 protein in relation to *Ucp1* and *Pgc1α* gene expression. It is well-established that phosphorylation of SIKs by LKB1 in the N-terminal kinase domain is essential for SIK activation, while phosphorylation by PKA in the internal regulatory domain results in SIK inhibition, which is no longer able to phosphorylate and exclude SIK substrates from nuclear accumulation [31; 32]. As a proof of concept, we constructed expression plasmids to delete the PKA phosphorylation domains alone (ΔPKA) or in combination with the kinase domain (ΔKD/PKA) (**Figure 3D**). We also constructed expression plasmids to mutate the S^{884} site into either phosphorylation-resistant S^{884A}, or phosphorylation-mimetic S^{884D} (**Figure 3D**). These SIK3 proteins with functional deletions or S^{884} mutations were re-expressed in *Sik3*-/- HIB-1B cells (clone SC19), and the effects on *Ucp1* and *Pgc1α* expression were evaluated. Consistent with our previous experiment (**Figure 2G**), re-expression of wild-type SIK3 protein significantly suppressed *Ucp1* expression after Iso stimulation (**Figure 3E**). More importantly, deletion of the internal PKA regulatory region in SIK3 confers resistance to PKA phosphorylation and results in constitutive suppression of *Ucp1* expression regardless of Iso stimulation, suggesting phosphorylation by PKA is essential for SIK3 inhibition to drive thermogenic gene expression (**Figure 3E**). In contrast, deletion of the kinase domain along with the PKA domain in SIK3 impairs its capacity to suppress *Ucp1* expression, suggesting that this effect depends on its kinase activity (**Figure 3E**). However, re-expression of either the phosphorylation-resistant SIK3 S^{884A} or the phosphorylation-mimetic SIK3 S^{884D} mutation does not change *Ucp1* expression, indicating that S^{884} phosphorylation alone does not alter the function of SIK3 in regulating *Ucp1* gene expression (**Figure 3E**). This finding suggests to us that mTORC1-dependent phosphorylation of SIK3 at S^{884} affects some other function in the overall βAR-dependent regulation of brown adipocytes that we have not yet considered. An unbiased approach in cells expressing the S^{884} mutants may yield new insight.

SIK inhibition *in vivo* by YKL-05-099 stimulates thermogenic gene expression and adipose browning

The SIK inhibitor YKL has been shown to be an effective inhibitor of SIK activity *in vivo* [48] and has been applied to disease models such as osteoporosis and leukemia [54; 55]. Our data showed that YKL can increase *Ucp1* gene expression in HIB-1B brown adipocyte *in vitro* (**Figure 2A**). We next sought to examine the effect of SIK inhibition by YKL on adipose tissue browning *in vivo*. A cohort of chow fed mice housed at room temperature was administered vehicle, YKL, or the β_3AR-agonist CL-316,243 as a positive control for adipose browning (**Figure 4A**). We measured both gene expression and histology of adipose tissues. YKL was dosed at 5, 10, and 20 mg/kg BW for 10 days. At all doses, it was well-tolerated without any obvious side effects except for a slight decrease in food-intake in the 20 mg group (data not shown). The mRNA levels of adipose browning marker genes *Ucp1*, *Pgc1α* and *Dio2* (iodothyronine deiodinase 2) were increased in the subcutaneous iWAT of mice treated with either the 10 mg or 20 mg doses of YKL (**Figure 4B**). In addition, UCP1 protein levels were also increased in the iWAT of 10 mg and 20 mg treatment groups (**Figure 4C**). Although the highest induction of UCP1 protein was observed in the 20 mg treatment group, the response was more consistent between individual mice in the 10 mg group (**Figure 4B and 4C**). The adipose tissue browning phenotype was confirmed by the appearance of UCP1-positive adipocytes in the iWAT of 10 mg and 20 mg treatment group with immunohistochemical staining. (**Figure 4D**). Taken together, these results demonstrate the potential of pharmacological SIK inhibition to improve adipose tissue browning *in vivo*.

HDAC4 is involved in SIK inhibition to promote thermogenic gene expression

Among those proteins that have been identified as SIK substrates, type IIa histone deacetylases (HDACs) and cAMP-regulated transcriptional coactivators (CRTCs) are the most well-studied [31; 32]. To determine whether type IIa HDACs are downstream mediators of SIK inhibition to drive *Ucp1* gene expression, we next tested the effect of class IIa HDAC inhibitors on *Ucp1* gene expression in HIB-1B brown adipocytes. Our results showed that class IIa HDAC inhibitors significantly reduced *Ucp1* gene expression after Iso stimulation (**Figure 5A**). In addition, knockdown of *Hdac4* in HIB-1B brown adipocytes blunted *Ucp1* gene expression upon SIK inhibition with the HG compound (**Figure 5B**). Similarly, knockdown of *Pgc1α*, a key regulator of *Ucp1* expression in brown adipocytes, also abolished *Ucp1* induction after SIK inhibition

(**Figure 5C**). These results suggested that SIK inhibition controls *Ucp1* gene expression potentially through the action of HDAC4.

As PGC1α is a master regulator of mitochondrial biogenesis and *Ucp1* expression in brown adipocytes, it has been shown that its deacetylation is required for its optimal coactivator activity [17]. Therefore, we next asked whether HDAC4-mediated PGC1α deacetylation could be a potential mechanism by which SIK inhibition could promote *Ucp1* gene expression. Consistent with a previous observation [56], our results showed that HDAC4 can be coimmunoprecipitated with PGC1α (**Figure 5D**). Of note, our data showed that β-adrenergic stimulation by Iso is required for the interaction of HDAC4 with PGC1α (**Figure 5E**). This is consistent with previously reports showing that cAMP signaling facilitates the nuclear translocation of HDAC4 [57; 58]. In addition, co-expression of HDAC4 can reduce the lysine acetylation of PGC1α (**Figure 5E**). We observed that lysine deacetylation seemed to increase the total PGC1α protein level (**Figure 5E**), indicating that lysine deacetylation might increase either PGC1α protein stability or prevent its degradation. Since the PGC1α antibody recognizes the C-terminal region of the protein, we do not know yet whether the deacetylation in this region will allow it to be better recognized by the antibody or not. Furthermore, we utilized mass spectrometry to determine which acetylated lysine(s) in PGC1α can be removed by HDAC4. Among several previously identified acetylation sites in PGC1α [19; 56], acetylated Lys183 (K183), K191, and K441 are significantly enriched in the control samples, but not in samples that co-express HDAC4 (**Figure 5F and 5G**). Note that the K183/K191 residues lie in the N-terminal transcriptional co-activation domain of PGC1α (**Figure 5F**), which raise the possibility that the coactivator activity of PGC1α might be potentiated by HDAC4-dependent lysine deacetylation.

Discussion

In this study, we identified SIK3 as a candidate substrate for mTORC1 in a SILAC screening for βAR-specific signaling in brown adipocytes. Our study defined a role for SIK3 as a suppressor of the brown adipocyte thermogenic gene program and showed that phosphorylation by PKA is essential for SIK3 inhibition to drive the thermogenic gene expression. Our study further demonstrated that pharmacological SIK inhibition promotes adipose tissue browning *in vivo*, even in the absence of a βAR stimulation, and suggests that SIK inhibition is a potential intervention

for metabolic diseases pending better mechanistic understanding. In addition, our study suggested that SIK inhibition stimulates the thermogenic program through the action of HDAC4, and this action might be linked to the deacetylation of PGC1α.

SIKs may play redundant roles in the regulation of the brown adipocyte thermogenic program

In line with previous reports [34; 40], our study also suggests that SIKs might play redundant roles in the regulation of the brown adipocyte thermogenic program. We showed that the pan-SIK inhibitors HG and YKL induce *Ucp1* expression in HIB-1B brown adipocytes without any additional βAR stimulation, and pharmacological SIK inhibition by YKL increases thermogenic gene expression and adipose browning *in vivo*. Global *Sik3* deletion disturbed glucose and lipid metabolism in mice [41], however, these phenotypes could be also caused by defects in other metabolically relevant tissues where they are expressed, such as the liver. Further characterization of a genetic model with adipose-specific *Sik3* deletion will be necessary to define its role in regulating adipose tissue metabolism *in vivo*.

The functional significance of SIK3 and mTORC1 interaction in adipocyte metabolism

Our study showed that SIK3 physically interacts with mTORC1 through RAPTOR. In line with this, a previous study also demonstrated that SIK3 can interact with several components of the mTOR complex, including RAPTOR [59]. Although that study was done in the context of bone development, both studies suggested a connection between SIK3 and mTOR complex, which might be applicable to the other tissue or organs as well. Our SILAC study showed that S^{884} in SIK3 is phosphorylated after Iso stimulation in a mTORC1-dependent manner. The functional significance of this SIK3-mTORC1 connection needs to be further explored in the context of adipocyte thermogenesis and metabolism perhaps by taking more unbiased approaches to uncover facets of SIK3 regulation of beige/brown adipocytes not yet known. Our data showed that phosphorylation of S^{884} in SIK3 by mTORC1 alone does not change its function in regulation of thermogenic gene expression (**Figure 3E**). This indicated that S^{884} is not by itself an essential functional phosphorylation site in SIK3, or it may function in synergy with other phosphorylation events to control SIK3 activity or its subcellular locations. In addition, our study demonstrated that SIK3 lacking an internal PKA regulatory domain is resistant to PKA-mediated SIK inhibition,

suggesting that phosphorylation by PKA is essential for SIK3 inhibition to drive the thermogenic gene expression after β-adrenergic stimulation.

Multi-layered regulation of PGC1α acetylation for brown adipocyte thermogenic program

PGC1α acetylation has been shown to be reversibly regulated by GCN5, SIRT1, and NAA10 and this regulation is a major mechanism for the control of PGC1α coactivator activity [18-20]. Our results support the notion that SIK inhibition stimulates thermogenic gene expression through the action of HDAC4. We showed that HDAC4 interacts with PGC1α after Iso stimulation, and HDAC4 catalyzes the deacetylation of PGC1α preferably in its transcriptional activation domain (**Figure 5**). Of note, another recent study also identified PGC1α as a new HDAC4 substrate for the control of skeletal muscle homeostasis [56]. This study showed that acetylated K328 in the PPARγ-interacting domain of PGC1α could be removed by HDAC4 [56], which might affect the interaction of PGC1α with PPARγ. This study, together with ours, suggest that HDAC4 might be a crucial regulator of PGC1α acetylation and function in metabolically active tissues such as the skeletal muscle and brown fat.

The translational potential of SIK inhibition to intervene in metabolic diseases

Several compounds have been reported as pan-SIK inhibitors, including HG-9-91-01 (HG) [46] and YKL-05-099 (YKL) [48]. And selective SIK inhibitors have also been developed, such as the SIK2-selective inhibitor ARN-3236 [60; 61], and the SIK3-selective inhibitor pterosin B (PTB) [49; 50]. Parenthetically, newer more selective and potent SIK3 inhibitors are currently in development [62]. Among these currently available inhibitors, SIK inhibition *in vivo* by YKL-05-099 has been shown to suppress acute myeloid leukemia progression [54], increase bone formation [55; 63], and modulate cytokine production [48]. Here our study showed that pharmacological SIK inhibition by YKL stimulates thermogenic gene expression and promotes adipose tissue browning *in vivo*. While it is unclear whether SIK inhibition in the adipose tissue alone or in other cell type(s) or tissue(s) contribute to the adipose tissue phenotypes and which SIK isoform is primarily responsible for this effect on adipose browning, the result is nevertheless encouraging from a target therapy perspective. It supports a role for SIK inhibition in adipose tissue and represents a potential intervention strategy that could be translated to obesity and cardiometabolic disease in future studies. Of note, a recent study showed that YKL can inhibit both SIKs and colony stimulating factor 1 receptor (CSF1R) to promote bone formation [63]. Although CSF1R inhibition has been

reported to result in reduced macrophage accumulation in adipose tissue [64], its role in the adipocyte thermogenic program is yet to be explored, and it is unclear whether CSF1R inhibition also plays a role for the adipose browning phenotypes in the YKL treated mice in our current study.

Methods

Reagents and antibodies

SIK inhibitors HG-9-91-01 (HG) (HY-101147), YKL-05-099 (YKL) (HY-15776), pterosin B (PTB) (HY-N1570), type IIa HDAC inhibitors TMP195 (HY-18361), TMP269 (HY-18360) were from MedChemExpress. Isoproterenol (Iso) (I6504), H-89 (B1427), puromycin (P8833), nicotinamide (NAM) (N0636) was from Sigma-Aldrich. Rapamycin (Rapa) (R-5000) was from LC Laboratories. Protease inhibitor (cOmplete Mini, 04693124001) and phosphatase inhibitor (PhosSTOP, 04906845001) cocktails were from Roche Diagnostics. The β3AR-selective agonist CL-316,243 (CL) was a gift from Elliott Danforth Jr. (American Cyanamid Co., Pearl River, New York, USA). Dulbecco's modified Eagle's medium (DMEM) (11995065), Penicillin-Streptomycin (15140122), insulin (Ins) (12585014) was from Gibco. Fatal bovine serum (FBS) was from CPS Serum (FBS-500-HI) or Atlas Biologicals (EF-0500-A). Rosiglitazone (Avandia) was from GlaxoSmithKline. Plasmocin (ant-mpp) was from InvivoGene. Polyethylenimine (PEI, 23966) was from Polysciences,

Anti-SIK3 (39477), Myc (2278 and 2276) and acetylated lysine (9441) antibodies were from Cell Signaling Technology. Anti-UCP1 antibody (ab23841) and mitochondrial OXPHOS antibody cocktail (ab110413) was form Abcam. Anti-PGC1α (A11971) antibody was from ABclonal. Anti-COXIV (11242-1-AP), β-actin (20536-I-AP) and GAPDH (10494-I-AP) antibodies were from ProteinTech. Anti-FLAG (A9469 and F1804), rabbit immunoglobulin G (IgG) (A3687), mouse IgG (A3562) antibodies, and anti-FLAG M2 antibody-conjugated affinity beads (A2220) were from Sigma-Aldrich.

Plasmids and constructs

The CMV-mSIK3-Myc-DDK-Neo (MR211912) plasmid were from Origene. The CMV-Raptor-Myc (1859), HDAC4-Flag (13821), pcDNA-f:PGC1 (1026), pCDNA4-myc-His-mPGC-1a (24925), pCAG-hHDAC4 (21096), pMSCVpuro-Gcn5 (63706), pEGFP-HDAC4 (45636),

pEGFP-HDAC4-3SA (45637), pLenti-Puro-sgSIK3-C (138683), pLenti-Puro-sgNT (138681), pLenti-CMV-GFP-Puro plasmid (17448), pLKO.1-puro (8453), pLKO.1-puro-scramble shRNA (1864) plasmids were from Addgene.

The CMV-mSIK3-3xFlag-Neo plasmid was constructed by subcloning of a 3xFlag tag to replace the Myc-DDK tag in the CMV-mSIK3-Myc-DDK-Neo plasmid. CMV-SIK3-3xFlag-Neo-ΔPKA was generated by BclI-digestion and relegation of CMV-mSIK3-3xFlag-Neo plasmid. CMV-SIK3-3xFlag-Neo-ΔKD/PKA was generated by NheI-digestion and relegation of CMV-mSIK3-3xFlag-Neo plasmid.

Lenti-mSIK3-3xFlag-Puro plasmid was constructed by subcloning the mSIK3-3xFlag coding sequences (CDS) from CMV-mSIK3-3xFlag-Neo plasmids to replace the GFP CDS in the pLenti-CMV-GFP-Puro plasmid. The Lenti-mSIK3-3xFlag-Puro plasmids with ΔPKA or ΔKD/PKA deletions were constructed with the same procedure.

The shRNA plasmids for *mSik3* were constructed by subcloning the annealed short hairpin oligos to the pLKO.1-puro vector as previously described [55]. The sequence of the short hairpins is CGCACGGAAGTTATGGAAGAT.

Cell lines

HEK293FT cells were from Invitrogen. HIB-1B brown adipocyte cells were a gift of Dr. Bruce Spiegelman. Cells were cultured in Growth Medium (DMEM with 10% FBS, 100 U/ml penicillin, 100 μg/ml streptomycin) supplemented with 25 μg/ml plasmocin. For differentiation, HIB-1B cells were induced with 1 μM rosiglitazone in Growth Medium for three to four days, and then maintained in Growth Medium overnight or until experiments.

SILAC phosphoproteomics study

Brown adipose tissue (BAT) cells were labeled with light (Arg0, Lys0), middle (Arg6, Lys4) and heavy (Arg10, Lys8) amino acids and starved for 12-16 h at 1% Fetal Calf Serum (FCS). The labeled cells were treated with insulin (10 nM), isoproterenol (1 μM) or rapamycin (100 nM). Rapamycin was pre-incubated for 30 min followed by the treatment with insulin or isoproterenol for 15 min. The middle-labeled cells were used as an internal standard. After treatment, cells were lysed with 500 μl 6 M guanidinium chloride. The light, middle and heavy lysates were mixed 1:1:1. Proteins were precipitated over night with 100% acetone followed by in-solution LysC digestion

and trypsin digestion overnight. After desalting, the sample peptides were separated with high pH-HPLC fractionation. The 12 pooled fractions were extracted two times with TiO2, and samples were put onto C8 stage tips (High-Select™ TiO2 Phosphopeptide Enrichment Kit; ThermoFisher), eluted, and then analyzed with a 90 min LC-MS/MS gradient at the Q Exactive mass spectrometer. The data was evaluated with MaxQuant and Perseus software. Every experiment was done in triplicate.

shRNA knockdown and SIK3 over-expression

HIB-1B cells were seeded in 6-well plate at a density of 5 x 10^5 cells/well and reached 90% confluence when ready for transfection the following day. Cells were transfected with 2.5 μg/well shRNA knockdown (pLKO.1-puro) or SIK3 expression (Lenti-mSIK3-3xFlag-Puro) plasmids by PEI reagent as previously described [65]. Six-hours after transfection, cells were induced for differentiation in Growth Medium with 1 μM rosiglitazone. Twenty-four hours after transfection, 3 μg/ml puromycin were added to the differentiation medium for drug selection for 2 days. Three or four days after differentiation, cells were supplemented with fresh Growth Medium and allowed to recover at lease for 3 hours before treatments for gene expression analysis.

CRISPR gene editing

HIB-1B cells were plated in 6-well plate at a density of 5 x 10^5 cells/well and reached 90% confluence when ready for transfection the following day. Cells were transfected with 2.5 μg/well pLenti-Puro-sgSIK3-C (SC) or pLenti-Puro-sgNT plasmids by PEI reagent according to standard protocol. Six-hours after transfection, cells were supplemented with Growth Medium. Twenty-four hours after transfection, 2 μg/ml puromycin were added to the medium for drug selection for 3 days. Cells were then supplemented with fresh Growth Medium, allowed to recover for 9 hours, trypsinized and replated in 96-well plate at a density of 1.6 cell/100ul/well. Single-cell clones were passaged and cryo-stored in liquid nitrogen. The genomic DNA were extracted from each clone with PureLink Genomic DNA Mini Kit (Invitrogen) and PCR amplified with the forward primer TCCCCTTCAGCTCTGTTCAG (mSik3-sgC-F1) and reverse primer AAGTGAAGTCTGGAGTGGGG (mSik3-sgC-R1). The PCR products were subcloned to T-vector (Promega) and sequenced. A pool of twelve single clones derived from the mock transfection of pLenti-Puro-sgNT plasmid were used as non-targeting control (NTC).

Mouse YKL treatment study

13-weeks-old male C57BL/6J mice were administrated vehicle (5% DMSO, 40% PEG300, 5% Tween-80, 50% Saline) or YKL at doses of 5, 10, and 20 mg/kg via intraperitoneal (i.p.) injection for 10 days. As a positive control, a group of mice were administrated β_3-AR selective agonist CL-316,243 at a dose of 1 mg/kg for 5 days. The food intake of each group was measured manually every day. All animal studies were approved by the Institutional Animal Care and Use Committee of Vanderbilt University Medical Center and in accordance with the NIH Guide for the Care and Use of Laboratory Animals.

Histology

Adipose tissues were fixed in 10% neutral buffered formaldehyde overnight, routinely processed for paraffin section, and stained with hematoxylin and eosin (H&E) or immunohistochemically stained for UCP1 (ab10983, Abcam). Histology was performed by the Vanderbilt Translational Pathology Shared Resource Core. Whole slides were imaged at 20x with a Leica SCN400 Slide Scanner by the Digital Histology Shared Resource Core at Vanderbilt University Medical Center.

QPCR

RNA was extracted with TRIzol (Invitrogen), purified with RNeasy Mini columns (Qiagen) or Quick-RNA columns (Zymo Research), and reversed transcribed with High-Capacity cDNA Reverse Transcription Kits (Applied Biosystems). QPCR was performed with *PowerUp* SYBR Green Master Mix (Life Technologies) per manufacturer's instruction. QPCR data were analyzed with the ΔΔCt method, normalized to the internal control gene 36B4, and presented as fold change relative to the control group.

Western blot

Protein was extracted as previously described [66]. In brief, adipose tissues were lysed and sonicated in Protein Lysis Buffer (25 mM HEPES, pH 7.4, 150 mM NaCl, 5 mM EDTA, 5 mM EGTA, 5 mM glycerophosphate, 0.9% Triton X-100, 0.1% IGEPAL, 5 mM sodium pyrophosphate, 10% glycerol, 1x cOmplete™ protease inhibitor cocktail and 1x PhoSTOP phosphatase inhibitors). For Western blotting, 30 to 40 μg of protein was resolved by 10% SDS-polyacrylamide gel electrophoresis, transferred to nitrocellulose membranes (Bio-Rad), incubated overnight at 4 °C with primary antibodies in blocking buffer (5% milk or bovine serum albumin in Tris-buffered saline, 0.1% Tween-20), and followed by inoculation with alkaline phosphatase–conjugated

secondary antibody for 1 hour at room temperature. Blots were incubated with Amersham ECF substrate (Cytiva, RPN5785) and images were acquired by Bio-Rad digital ChemiDoc MP with IR (VUMC Molecular Cell Biology Resource).

Immunoprecipitation

HEK293FT cells were plated in 6-well plate at a density of 6 x 10^5 cells/well, transfected with 2.5 μg/well of indicated plasmids on the following day, and harvested for protein lysate 24 hours after transfection. For immunoprecipitation, 300-500 μg protein lysates were incubated with 15 μl of anti-FLAG M2 Affinity Gel (Sigma, A2220) in Protein Lysis Buffer at 4 °C for 2 hours. Affinity agarose beads were washed and eluted with 20 μl 2x NuPAGE LDS sample buffer (Invitrogen, NP0008) by incubation at 95 °C for 5 min. Protein eluent were subjected to SDS-PAGE gel and Western blot analysis as described above.

PGC1α acetylation and mass spectrometry

HEK293FT cells were plated in 10-cm plate at a density of 3 x 10^6 cells/plate, and on the following day transfected with 15 μg plasmids/plate, including mPGC1a-Flag, pMSCVpuro-GCN5, hNAA10-Myc-His, with or without pCAG-hHDAC4. Cells were supplemented with fresh medium 6 hours after transfection, treated with 5 mM nicotinamide overnight and with 1 μM isoproterenol for 6 hours the following day, and lysed in 1x Cell Lysis Buffer (CST, 9803) supplemented with 1x cOmplete™ protease inhibitor cocktail and 1x PhoSTOP phosphatase inhibitors. For Western blot analysis of PGC1α acetylation, 500 μg protein lysate were used for immunoprecipitation as described above. For mass spectrometry analysis, 2 mg protein lysates were incubated overnight at 4 °C with 50 μl of anti-FLAG M2 Affinity Gel in a total of 1.2 ml 1x Cell Lysis Buffer (CST, 9803) supplemented with 1x cOmplete™ protease inhibitor cocktail and 1x PhoSTOP phosphatase inhibitors. Affinity agarose beads were washed and eluted twice with 45 μl 2x Leammli sample buffer (Sigma, S3401) by incubation at 95 °C for 5 min. Elutes were resolved by SDS-PAGE electrophoresis and stained by Bio-Safe™ Coomassie G-250 (BioRad #1610786).

The downstream LC-MS analysis was done at Vanderbilt Mass Spectrometry Research Core Lab. In brief, Coomassie stained protein band were cut out and in-gel digested by trypsin overnight. The trypsinized peptides were subjected to LC-MS analysis to determine the level of lysine acetylation. Lysine acetylation in target peptides is normalized with two reference peptides (YDSYEAYEHER and DDGDSYGFITYR) and the average fold changes were presented.

Statistical analysis

GraphPad Prism and Microsoft Excel was used for statistical analysis. All data were presented as means ± SEM. Unpaired two-tailed Student's t-tests were used to determine the differences between groups. Statistical significance was defined as $p < 0.05$.

Acknowledgement

We thank Dr. Noriyuki Tsumaki from Kyoto University for providing the *Sik3* floxed mice, Ms. Wei Zhang for excellent technical assistance and animal husbandry. This work was supported by NIH R01 DK116625 (S.C.).

Figure Legends

Figure 1. Phosphoproteomic analysis identified a mTORC1 phosphorylation site in salt-inducible kinase 3.

(A) BAT adipocytes labeling and treatment for SILAC analysis. BAT adipocytes were labeled with light (Arg0, Lys0), middle (Arg6, Lys4) and heavy (Arg10, Lys8) amino acids, pretreated with rapamycin (Rapa) for 30 min, and then treated with isoproterenol (Iso) or insulin (Ins) for 15 min. Cell lysates were processed and subjected to liquid chromatography and mass spectrometry analysis to profile the phosphorylated peptides.

(B) Representative phosphoproteins whose phosphorylation is increased by isoproterenol (Iso. blue) or insulin (Ins, orange) and blocked by rapamycin (Rapa, green).

(C) The phosphorylation of S6 Ser^{240}, AKT Ser^{473} and SIK3 Ser^{884} in response to Iso, Ins and Rapa treatment. Data are Log2 fold change compared to the vehicle treated samples. *$p<0.05$.

(D) SIK protein structure and phosphorylation sites. The LKB1 (Liver kinase B1, orange), PKA (blue), and mTORC1 (S884, red) phosphorylation sites are as indicated. KD: kinase domain. UBA: ubiquitin-associated domain.

(E) Flag-tagged SIK3 and Myc-tagged RAPTOR were expressed in 293FT cells. Protein lysates were immunoprecipitated with Flag beads and analyzed by Western blot.

Figure 2. SIK inhibition stimulates thermogenic gene expression in brown adipocyte.

(A-B) SIK inhibitors HG-9-91-01 (HG) and YKL-05-099 (YKL) increase *Ucp1* expression in a dose-dependent manner in HIB-1B brown adipocytes.

(C-D) SIK inhibition by HG (1μM) restores the suppression of *Ucp1* expression by mTORC1 (Rapa, 100nM) or PKA (H89, 20μM) blockades in HIB-1B brown adipocytes.

(E) shRNA knockdown (KD) of *Sik3* increases *Ucp1* expression in HIB-1B brown adipocytes.

(F) Overexpression (OE) of SIK3 reduces *Ucp1* expression in HIB-1B brown adipocytes.

Iso: 100nM for 3hr. Student's t-test, *p<0.05, **p<0.01, ***p<0.001, ****<0.0001, ns: no statistical significance.

Figure 3. *Sik3* deletion in brown adipocytes increases thermogenic gene expression.

(A) Sequence of wild-type and CRISPR-edited *Sik3* mutations, the guide RNA (gRNA), and the protospacer adjacent motif (PAM) are showed (upper). The wild-type non-targeting control (NTC), and two CRISPR-edited HIB-1B clones with frame-shifted *Sik3* mutations (SC19 and SC13) are generated (lower).

(B) Expression of SIK3, PGC1α and mitochondrial OXPHOS proteins in control and *Sik3*-/- brown adipocytes.

(C) Expression of *Sik3*, *Ucp1* and *Pgc1α* mRNA in control and *Sik3*-/- brown adipocytes. Student's t-test, **p<0.01, ***p<0.001, ****p<0.0001 vs NTC at baseline (vehicle). $^{\#}$p<0.01, $^{\#\#\#}$p<0.001, $^{\#\#\#\#}$p<0.0001 vs NTC after isoproterenol (Iso) stimulation.

(D) SIK3 deletion constructs. ΔPKA: Δ432-805, deletion of the regulatory PKA phosphorylation domain. ΔKD/PKA: Δ147-850, deletion of kinase domain (KD), ubiquitin-associated domain (UBA), and the regulatory PKA phosphorylation domain.

(E) Expression of *Ucp1* mRNA in *Sik3*-/- brown adipocytes (SC19) transfected with GFP, SIK3, and SIK3 deletion plasmids. Student's t-test, ***p<0.001, ****p<0.0001.

Figure 4. SIK inhibition by YKL-05-099 promotes adipose tissue browning *in vivo*.

(A) YKL-05-099 (YKL) was i.p. injected daily at 5, 10, and 20 mg/kg bodyweight (YKL5, 10, 20) for 10 days. β_3-AR agonist CL-316,243 (CL) was i.p. injected daily at 1 mg/kg bodyweight for 5 days as positive control (left). Representative images of inguinal white adipose tissues (iWAT) were showed (right).

(B) QPCR analysis of *Ucp1*, *Pgc1α* and *Dio2* mRNA expression in iWAT. Student's t-test, *p<0.05, **p<0.01, ***p<0.001.

(C) Western blot analysis of UCP1 protein expression in iWAT (left). Red asterisks indicate the non-specific bands. Quantification of UCP1 protein in Western blot (right).

(D) Immunohistochemistry staining of UCP1 protein in iWAT.

Figure 5. HDAC4 is involved in SIK inhibition to promote thermogenic gene expression.

(A) Class IIa HDAC inhibitors Tmp195 and Tmp269 blunt Iso-stimulated Ucp1 expression.

(B-C) *Hdac4* or *Pgc1α* knockdown blunts the increase of *Ucp1* expression upon SIK inhibition. ****p<0.0001; ***p< 0.001; **p<0.01; *p<0.05.

(D) HDAC4 interacts with PGC1α. HEK293FT cells were transiently transfected with indicated plasmids and treated with 1 μM Iso for 6 hrs.

(E) mPGC1α-Flag, mGCN5, hNAA10-myc plasmids were co-transfected either with hHDAC4 or vector into HEK293FT cells. PGC1α were pulled down with a Flag-beads for Western blot analysis of lysine acetylation (Acetyl-Lys).

(F) The functional domain and acetylated lysine sites in PGC1α.

(G) Enrichment of acetylated lysine (Acetyl-Lys) in PGC1α. Immunoprecipitated PGC1α were subjected to quantitative mass spectrometry analysis to determine the lysine acetylation level. The acetylation of K183, K191 and K441 were reduced in cells that do express HDAC4.

References

[1] Wang, Y.C., McPherson, K., Marsh, T., Gortmaker, S.L., Brown, M., 2011. Health and economic burden of the projected obesity trends in the USA and the UK. Lancet 378(9793):815-825.

[2] Walden, T.B., Hansen, I.R., Timmons, J.A., Cannon, B., Nedergaard, J., 2012. Recruited vs. nonrecruited molecular signatures of brown, "brite," and white adipose tissues. Am J Physiol Endocrinol Metab 302(1):E19-31.

[3] Wu, J., Bostrom, P., Sparks, L.M., Ye, L., Choi, J.H., Giang, A.H., et al., 2012. Beige adipocytes are a distinct type of thermogenic fat cell in mouse and human. Cell 150(2):366-376.

[4] Guerra, C., Koza, R.A., Yamashita, H., Walsh, K., Kozak, L.P., 1998. Emergence of brown adipocytes in white fat in mice is under genetic control. Effects on body weight and adiposity. J Clin Invest 102(2):412-420.

[5] Vernochet, C., Peres, S.B., Davis, K.E., McDonald, M.E., Qiang, L., Wang, H., et al., 2009. C/EBPalpha and the corepressors CtBP1 and CtBP2 regulate repression of select visceral white adipose genes during induction of the brown phenotype in white adipocytes by peroxisome proliferator-activated receptor gamma agonists. Mol Cell Biol 29(17):4714-4728.

[6] Petrovic, N., Walden, T.B., Shabalina, I.G., Timmons, J.A., Cannon, B., Nedergaard, J., 2010. Chronic peroxisome proliferator-activated receptor gamma (PPARgamma) activation of epididymally derived white adipocyte cultures reveals a population of thermogenically competent, UCP1-containing adipocytes molecularly distinct from classic brown adipocytes. J Biol Chem 285(10):7153-7164.

[7] Collins, S., Petro, A.E., Surwit, R.S., 1997. Strain-specific response to b_3-adrenergic receptor agonist treatment of diet-induced obesity in mice. Endocrinology 138:405-413.

[8] Cypess, A.M., Lehman, S., Williams, G., Tal, I., Rodman, D., Goldfine, A.B., et al., 2009. Identification and importance of brown adipose tissue in adult humans. N Engl J Med 360(15):1509-1517.

[9] van Marken Lichtenbelt, W.D., Vanhommerig, J.W., Smulders, N.M., Drossaerts, J.M., Kemerink, G.J., Bouvy, N.D., et al., 2009. Cold-activated brown adipose tissue in healthy men. N Engl J Med 360(15):1500-1508.

[10] Virtanen, K.A., Lidell, M.E., Orava, J., Heglind, M., Westergren, R., Niemi, T., et al., 2009. Functional brown adipose tissue in healthy adults. N Engl J Med 360(15):1518-1525.

[11] Rosen, E.D., Spiegelman, B.M., 2014. What we talk about when we talk about fat. Cell 156(1-2):20-44.

[12] Stanford, K.I., Middelbeek, R.J., Townsend, K.L., An, D., Nygaard, E.B., Hitchcox, K.M., et al., 2013. Brown adipose tissue regulates glucose homeostasis and insulin sensitivity. J Clin Invest 123(1):215-223.

[13] Becher, T., Palanisamy, S., Kramer, D.J., Eljalby, M., Marx, S.J., Wibmer, A.G., et al., 2021. Brown adipose tissue is associated with cardiometabolic health. Nat Med 27(1):58-65.

[14] Shi, F., Collins, S., 2017. Second messenger signaling mechanisms of the brown adipocyte thermogenic program: an integrative perspective. Horm Mol Biol Clin Investig 31(2).

[15] Inagaki, T., Sakai, J., Kajimura, S., 2016. Transcriptional and epigenetic control of brown and beige adipose cell fate and function. Nat Rev Mol Cell Biol 17(8):480-495.

[16] Lin, J., Handschin, C., Spiegelman, B.M., 2005. Metabolic control through the PGC-1 family of transcription coactivators. Cell Metab 1(6):361-370.

[17] Jeninga, E.H., Schoonjans, K., Auwerx, J., 2010. Reversible acetylation of PGC-1: connecting energy sensors and effectors to guarantee metabolic flexibility. Oncogene 29(33):4617-4624.

[18] Lerin, C., Rodgers, J.T., Kalume, D.E., Kim, S.H., Pandey, A., Puigserver, P., 2006. GCN5 acetyltransferase complex controls glucose metabolism through transcriptional repression of PGC-1alpha. Cell Metab 3(6):429-438.

[19] Rodgers, J.T., Lerin, C., Haas, W., Gygi, S.P., Spiegelman, B.M., Puigserver, P., 2005. Nutrient control of glucose homeostasis through a complex of PGC-1alpha and SIRT1. Nature 434(7029):113-118.

[20] Lee, C.C., Shih, Y.C., Kang, M.L., Chang, Y.C., Chuang, L.M., Devaraj, R., et al., 2019. Naa10p Inhibits Beige Adipocyte-Mediated Thermogenesis through N-alpha-acetylation of Pgc1alpha. Mol Cell 76(3):500-515 e508.
[21] Wang, Q., Kajimura, S., 2019. Naa10P puts a brake on PGC1alpha and fat browning. Nat Struct Mol Biol 26(10):849-851.
[22] Cao, W., Daniel, K.W., Robidoux, J., Puigserver, P., Medvedev, A.V., Bai, X., et al., 2004. p38 mitogen-activated protein kinase is the central regulator of cyclic AMP-dependent transcription of the brown fat uncoupling protein 1 gene. Mol Cell Biol 24(7):3057-3067.
[23] Cao, W., Medvedev, A.V., Daniel, K.W., Collins, S., 2001. beta-Adrenergic activation of p38 MAP kinase in adipocytes: cAMP induction of the uncoupling protein 1 (UCP1) gene requires p38 MAP kinase. J Biol Chem 276(29):27077-27082.
[24] Robidoux, J., Cao, W., Quan, H., Daniel, K.W., Moukdar, F., Bai, X., et al., 2005. Selective activation of mitogen-activated protein (MAP) kinase kinase 3 and p38alpha MAP kinase is essential for cyclic AMP-dependent UCP1 expression in adipocytes. Mol Cell Biol 25(13):5466-5479.
[25] Liu, D., Bordicchia, M., Zhang, C., Fang, H., Wei, W., Li, J.L., et al., 2016. Activation of mTORC1 is essential for beta-adrenergic stimulation of adipose browning. J Clin Invest 126(5):1704-1716.
[26] Guilherme, A., Yenilmez, B., Bedard, A.H., Henriques, F., Liu, D., Lee, A., et al., 2020. Control of Adipocyte Thermogenesis and Lipogenesis through β3-Adrenergic and Thyroid Hormone Signal Integration. Cell Rep 31(5):107598.
[27] Tran, C.M., Mukherjee, S., Ye, L., Frederick, D.W., Kissig, M., Davis, J.G., et al., 2016. Rapamycin Blocks Induction of the Thermogenic Program in White Adipose Tissue. Diabetes 65(4):927-941.
[28] García-Casarrubios, E., de Moura, C., Arroba, A.I., Pescador, N., Calderon-Dominguez, M., Garcia, L., et al., 2016. Rapamycin negatively impacts insulin signaling, glucose uptake and uncoupling protein-1 in brown adipocytes. Biochim Biophys Acta 1861(12 Pt A):1929-1941.
[29] Liu, D., Ceddia, R.P., Collins, S., 2018. Cardiac natriuretic peptides promote adipose 'browning' through mTOR complex-1. Mol Metab 9:192-198.
[30] Xu, Y., Shi, T., Cui, X., Yan, L., Wang, Q., Xu, X., et al., 2021. Asparagine reinforces mTORC1 signaling to boost thermogenesis and glycolysis in adipose tissues. EMBO J 40(24):e108069.
[31] Wein, M.N., Foretz, M., Fisher, D.E., Xavier, R.J., Kronenberg, H.M., 2018. Salt-Inducible Kinases: Physiology, Regulation by cAMP, and Therapeutic Potential. Trends Endocrinol Metab 29(10):723-735.
[32] Sakamoto, K., Bultot, L., Goransson, O., 2018. The Salt-Inducible Kinases: Emerging Metabolic Regulators. Trends Endocrinol Metab 29(12):827-840.
[33] Sonntag, T., Vaughan, J.M., Montminy, M., 2018. 14-3-3 proteins mediate inhibitory effects of cAMP on salt-inducible kinases (SIKs). FEBS J 285(3):467-480.
[34] Wang, Y., Paulo, E., Wu, D., Wu, Y., Huang, W., Chawla, A., et al., 2017. Adipocyte Liver Kinase b1 Suppresses Beige Adipocyte Renaissance Through Class IIa Histone Deacetylase 4. Diabetes 66(12):2952-2963.
[35] Sall, J., Pettersson, A.M., Bjork, C., Henriksson, E., Wasserstrom, S., Linder, W., et al., 2017. Salt-inducible kinase 2 and -3 are downregulated in adipose tissue from obese or insulin-resistant individuals: implications for insulin signalling and glucose uptake in human adipocytes. Diabetologia 60(2):314-323.
[36] Muraoka, M., Fukushima, A., Viengchareun, S., Lombes, M., Kishi, F., Miyauchi, A., et al., 2009. Involvement of SIK2/TORC2 signaling cascade in the regulation of insulin-induced PGC-1alpha and UCP-1 gene expression in brown adipocytes. Am J Physiol Endocrinol Metab 296(6):E1430-1439.
[37] Park, J., Yoon, Y.S., Han, H.S., Kim, Y.H., Ogawa, Y., Park, K.G., et al., 2014. SIK2 is critical in the regulation of lipid homeostasis and adipogenesis in vivo. Diabetes 63(11):3659-3673.
[38] Horike, N., Takemori, H., Katoh, Y., Doi, J., Min, L., Asano, T., et al., 2003. Adipose-specific expression, phosphorylation of Ser794 in insulin receptor substrate-1, and activation in diabetic animals of salt-inducible kinase-2. J Biol Chem 278(20):18440-18447.

[39] Du, J., Chen, Q., Takemori, H., Xu, H., 2008. SIK2 can be activated by deprivation of nutrition and it inhibits expression of lipogenic genes in adipocytes. Obesity (Silver Spring) 16(3):531-538.
[40] Paulo, E., Wu, D., Wang, Y., Zhang, Y., Wu, Y., Swaney, D.L., et al., 2018. Sympathetic inputs regulate adaptive thermogenesis in brown adipose tissue through cAMP-Salt inducible kinase axis. Sci Rep 8(1):11001.
[41] Uebi, T., Itoh, Y., Hatano, O., Kumagai, A., Sanosaka, M., Sasaki, T., et al., 2012. Involvement of SIK3 in glucose and lipid homeostasis in mice. PLoS One 7(5):e37803.
[42] Shan, T., Xiong, Y., Zhang, P., Li, Z., Jiang, Q., Bi, P., et al., 2016. Lkb1 controls brown adipose tissue growth and thermogenesis by regulating the intracellular localization of CRTC3. Nat Commun 7:12205.
[43] Hsu, P.P., Kang, S.A., Rameseder, J., Zhang, Y., Ottina, K.A., Lim, D., et al., 2011. The mTOR-regulated phosphoproteome reveals a mechanism of mTORC1-mediated inhibition of growth factor signaling. Science 332(6035):1317-1322.
[44] Hara, K., Maruki, Y., Long, X., Yoshino, K., Oshiro, N., Hidayat, S., et al., 2002. Raptor, a binding partner of target of rapamycin (TOR), mediates TOR action. Cell 110(2):177-189.
[45] Kim, D.H., Sarbassov, D.D., Ali, S.M., King, J.E., Latek, R.R., Erdjument-Bromage, H., et al., 2002. mTOR interacts with raptor to form a nutrient-sensitive complex that signals to the cell growth machinery. Cell 110(2):163-175.
[46] Clark, K., MacKenzie, K.F., Petkevicius, K., Kristariyanto, Y., Zhang, J., Choi, H.G., et al., 2012. Phosphorylation of CRTC3 by the salt-inducible kinases controls the interconversion of classically activated and regulatory macrophages. Proc Natl Acad Sci U S A 109(42):16986-16991.
[47] Wang, H., Willershauser, M., Karlas, A., Gorpas, D., Reber, J., Ntziachristos, V., et al., 2019. A dual Ucp1 reporter mouse model for imaging and quantitation of brown and brite fat recruitment. Mol Metab 20:14-27.
[48] Sundberg, T.B., Liang, Y., Wu, H., Choi, H.G., Kim, N.D., Sim, T., et al., 2016. Development of Chemical Probes for Investigation of Salt-Inducible Kinase Function in Vivo. ACS Chem Biol 11(8):2105-2111.
[49] Itoh, Y., Sanosaka, M., Fuchino, H., Yahara, Y., Kumagai, A., Takemoto, D., et al., 2015. Salt-inducible Kinase 3 Signaling Is Important for the Gluconeogenic Programs in Mouse Hepatocytes. J Biol Chem 290(29):17879-17893.
[50] Yahara, Y., Takemori, H., Okada, M., Kosai, A., Yamashita, A., Kobayashi, T., et al., 2016. Pterosin B prevents chondrocyte hypertrophy and osteoarthritis in mice by inhibiting Sik3. Nat Commun 7:10959.
[51] Hollstein, P.E., Eichner, L.J., Brun, S.N., Kamireddy, A., Svensson, R.U., Vera, L.I., et al., 2019. The AMPK-Related Kinases SIK1 and SIK3 Mediate Key Tumor-Suppressive Effects of LKB1 in NSCLC. Cancer Discov 9(11):1606-1627.
[52] Baker, K.E., Parker, R., 2004. Nonsense-mediated mRNA decay: terminating erroneous gene expression. Curr Opin Cell Biol 16(3):293-299.
[53] Fu, Y., Foden, J.A., Khayter, C., Maeder, M.L., Reyon, D., Joung, J.K., et al., 2013. High-frequency off-target mutagenesis induced by CRISPR-Cas nucleases in human cells. Nat Biotechnol 31(9):822-826.
[54] Tarumoto, Y., Lin, S., Wang, J., Milazzo, J.P., Xu, Y., Lu, B., et al., 2020. Salt-inducible kinase inhibition suppresses acute myeloid leukemia progression in vivo. Blood 135(1):56-70.
[55] Wein, M.N., Liang, Y., Goransson, O., Sundberg, T.B., Wang, J., Williams, E.A., et al., 2016. SIKs control osteocyte responses to parathyroid hormone. Nat Commun 7:13176.
[56] Luo, L., Martin, S.C., Parkington, J., Cadena, S.M., Zhu, J., Ibebunjo, C., et al., 2019. HDAC4 Controls Muscle Homeostasis through Deacetylation of Myosin Heavy Chain, PGC-1alpha, and Hsc70. Cell Rep 29(3):749-763 e712.
[57] Walkinshaw, D.R., Weist, R., Xiao, L., Yan, K., Kim, G.W., Yang, X.J., 2013. Dephosphorylation at a conserved SP motif governs cAMP sensitivity and nuclear localization of class IIa histone deacetylases. J Biol Chem 288(8):5591-5605.

[58] McKinsey, T.A., Zhang, C.L., Olson, E.N., 2001. Identification of a signal-responsive nuclear export sequence in class II histone deacetylases. Mol Cell Biol 21(18):6312-6321.
[59] Csukasi, F., Duran, I., Barad, M., Barta, T., Gudernova, I., Trantirek, L., et al., 2018. The PTH/PTHrP-SIK3 pathway affects skeletogenesis through altered mTOR signaling. Sci Transl Med 10(459).
[60] Lombardi, M.S., Gilliéron, C., Dietrich, D., Gabay, C., 2016. SIK inhibition in human myeloid cells modulates TLR and IL-1R signaling and induces an anti-inflammatory phenotype. J Leukoc Biol 99(5):711-721.
[61] Zhou, J., Alfraidi, A., Zhang, S., Santiago-O'Farrill, J.M., Yerramreddy Reddy, V.K., Alsaadi, A., et al., 2017. A Novel Compound ARN-3236 Inhibits Salt-Inducible Kinase 2 and Sensitizes Ovarian Cancer Cell Lines and Xenografts to Paclitaxel. Clin Cancer Res 23(8):1945-1954.
[62] António, T., Soares-da-Silva, P., Pires, N.M., Gomes, P., 2022. Salt-inducible kinases: new players in pulmonary arterial hypertension? Trends Pharmacol Sci 43(10):806-819.
[63] Tang, C.C., Castro Andrade, C.D., O'Meara, M.J., Yoon, S.H., Sato, T., Brooks, D.J., et al., 2021. Dual targeting of salt inducible kinases and CSF1R uncouples bone formation and bone resorption. Elife 10.
[64] Merry, T.L., Brooks, A.E.S., Masson, S.W., Adams, S.E., Jaiswal, J.K., Jamieson, S.M.F., et al., 2020. The CSF1 receptor inhibitor pexidartinib (PLX3397) reduces tissue macrophage levels without affecting glucose homeostasis in mice. Int J Obes (Lond) 44(1):245-253.
[65] Shi, F., Simandi, Z., Nagy, L., Collins, S., 2021. Diet-dependent natriuretic peptide receptor C expression in adipose tissue is mediated by PPARγ via long-range distal enhancers. J Biol Chem 297(2):100941.
[66] Wu, W., Shi, F., Liu, D., Ceddia, R.P., Gaffin, R., Wei, W., et al., 2017. Enhancing natriuretic peptide signaling in adipose tissue, but not in muscle, protects against diet-induced obesity and insulin resistance. Sci Signal 10(489).

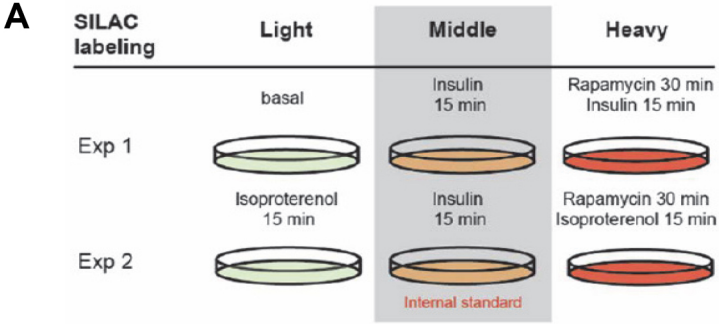
A
SILAC labeling
Light
Middle
Heavy
basal
Insulin 15 min
Rapamycin 30 min Insulin 15 min
Exp 1
Isoproterenol 15 min
Insulin 15 min
Rapamycin 30 min Isoproterenol 15 min
Exp 2
Internal standard

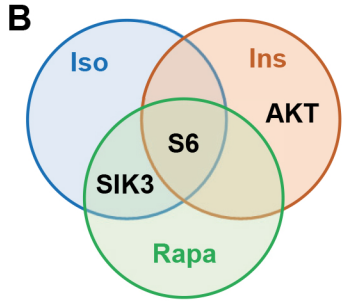
B
Iso
Ins
AKT
S6
SIK3
Rapa

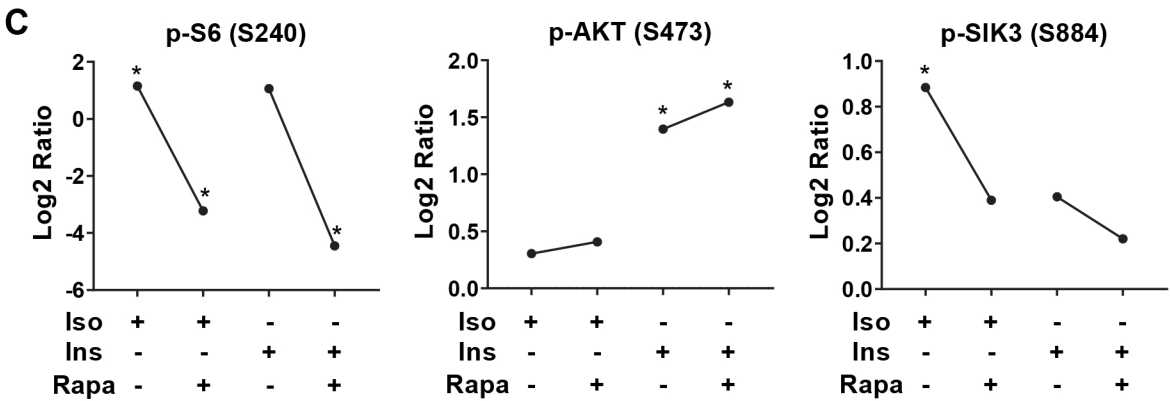
C
p-S6 (S240)
p-AKT (S473)
p-SIK3 (S884)
Log2 Ratio
Iso
Ins
Rapa

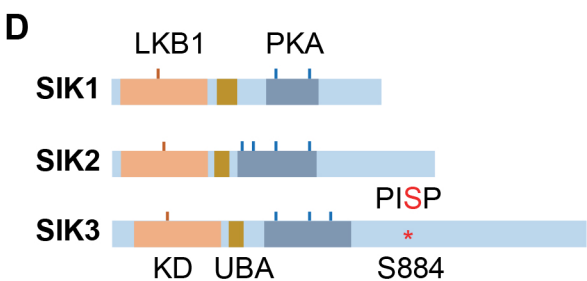
D
LKB1
PKA
SIK1
SIK2
PISP
SIK3
KD
UBA
S884

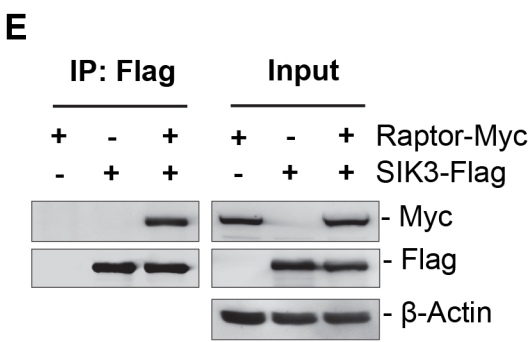
E
IP: Flag
Input
Raptor-Myc
SIK3-Flag
- Myc
- Flag
- β-Actin

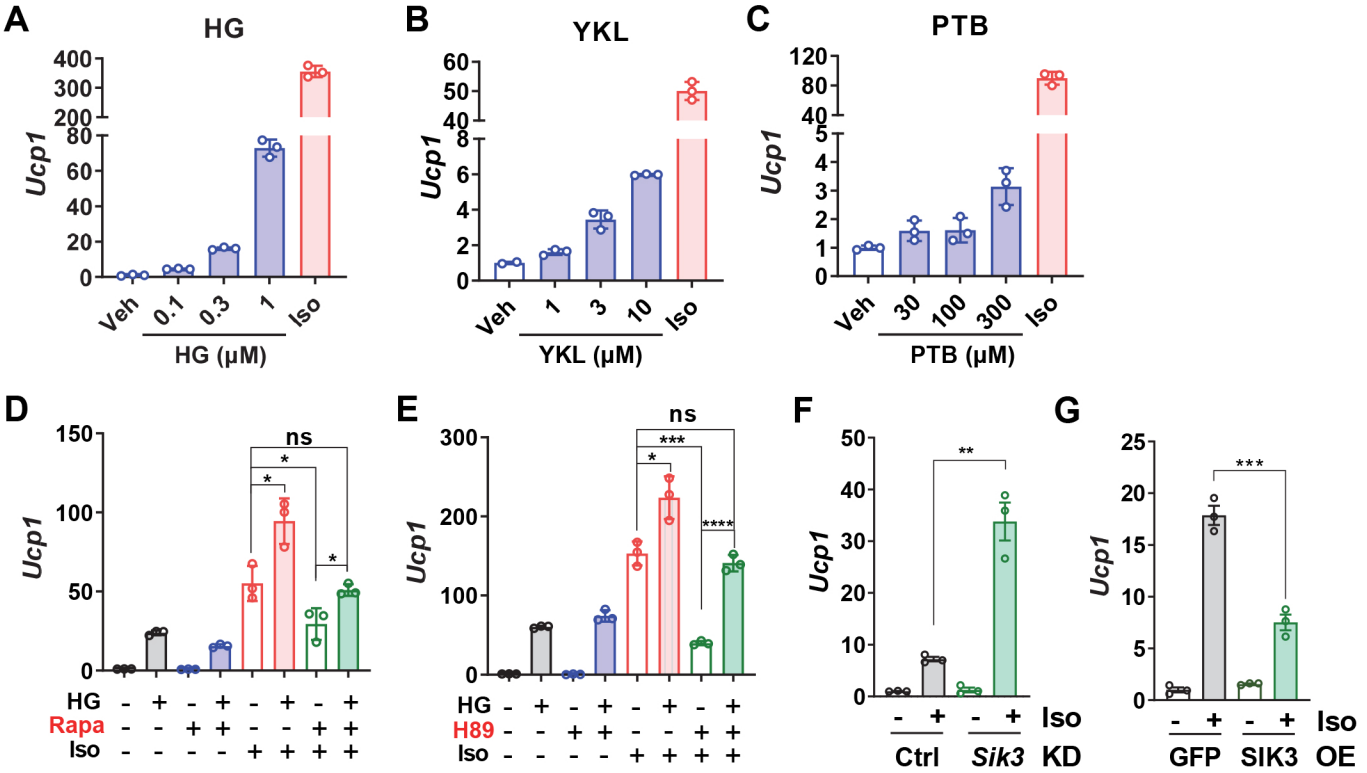
A
HG
Ucp1
400
300
200
80
60
40
20
0
Veh
0.1
0.3
1
Iso
HG (μM)
B
YKL
Ucp1
60
50
40
8
6
4
2
0
Veh
1
3
10
Iso
YKL (μM)
C
PTB
Ucp1
120
80
40
5
4
3
2
1
0
Veh
30
100
300
Iso
PTB (μM)
D
Ucp1
150
100
50
0
ns
*
*
*
HG - + - + - + - +
Rapa - - + + - - + +
Iso - - - - + + + +
E
Ucp1
300
200
100
0
ns
***
*
****
HG - + - + - + - +
H89 - - + + - - + +
Iso - - - - + + + +
F
Ucp1
50
40
30
20
10
0
**
- + - + Iso
Ctrl Sik3 KD
G
Ucp1
25
20
15
10
5
0
***
- + - + Iso
GFP SIK3 OE

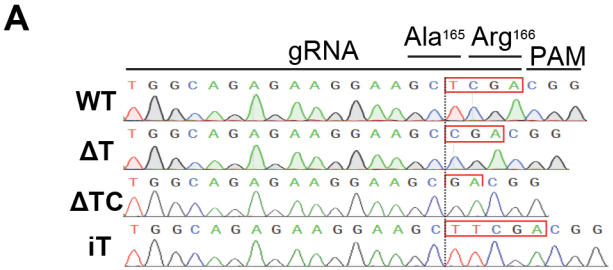

Clones	CRISPR	CDS
NTC	None	Wild-type
SC19	ΔTC/iT	Frame-shift
SC13	ΔT/iT	Frame-shift

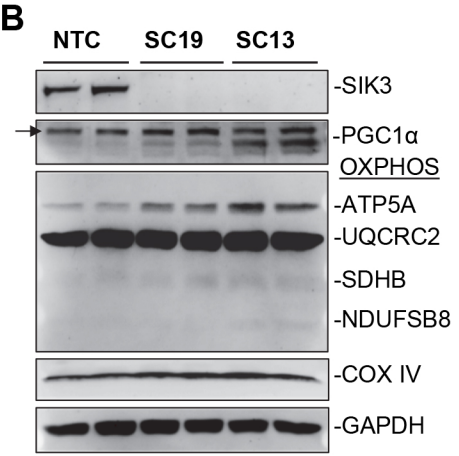

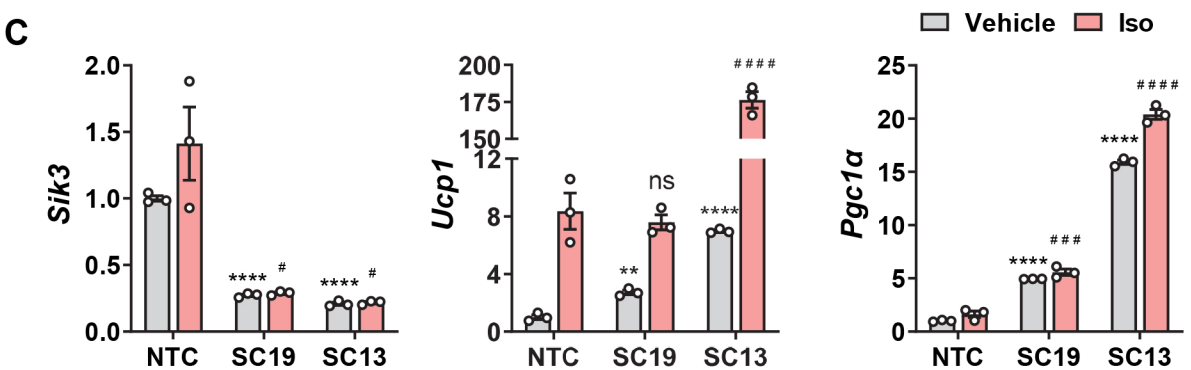

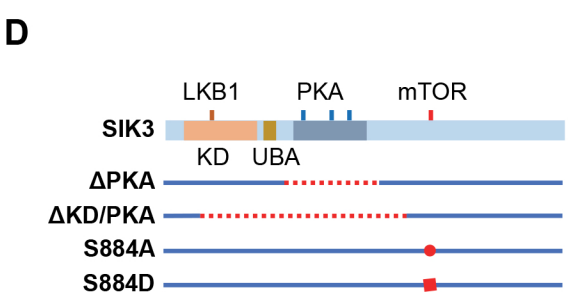

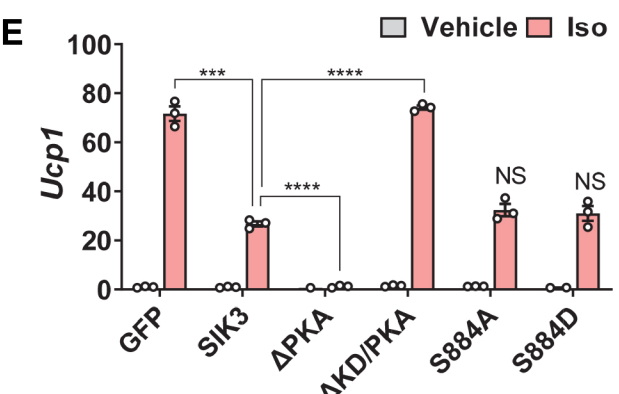

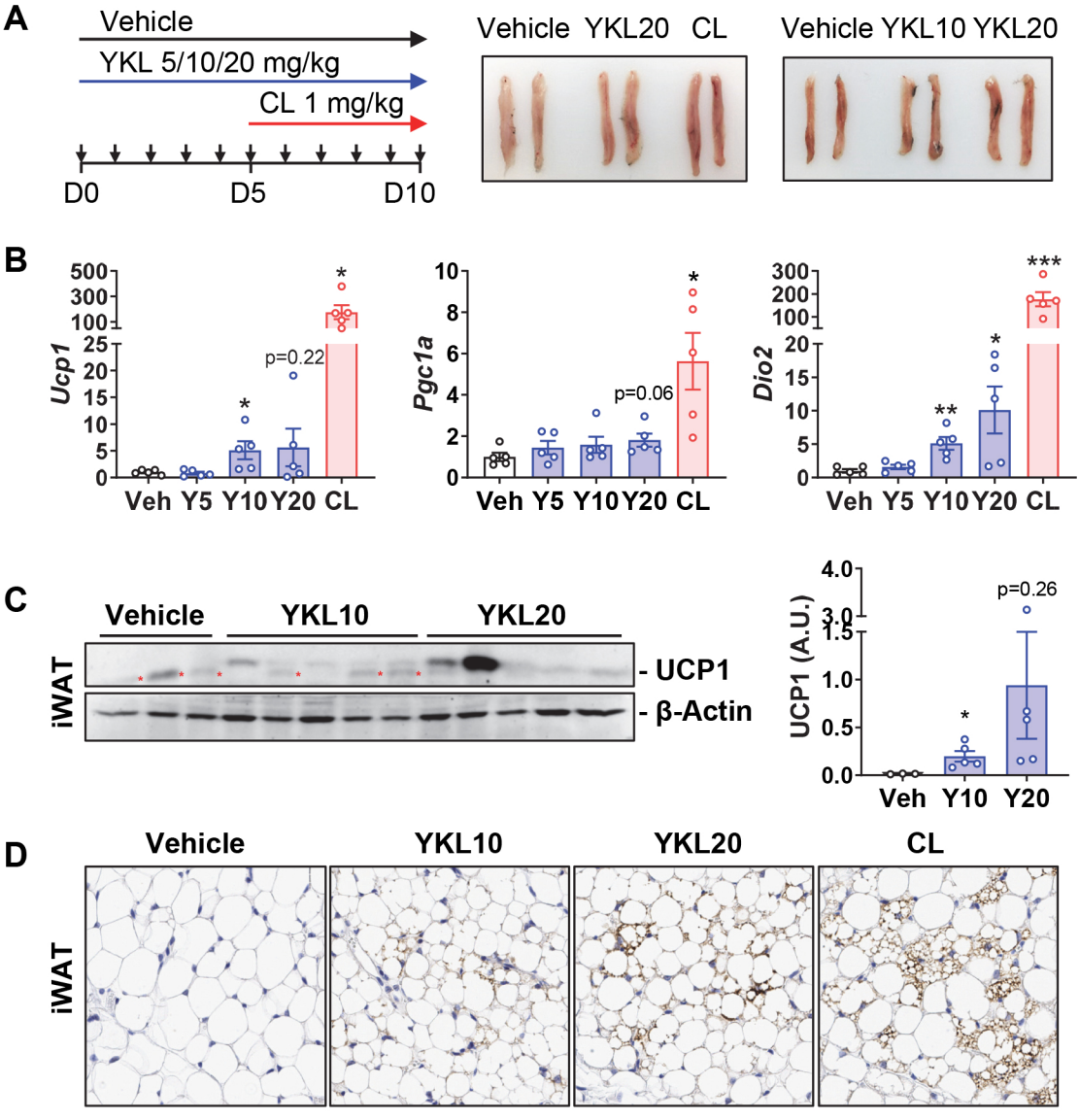
A
Vehicle
YKL 5/10/20 mg/kg
CL 1 mg/kg
D0
D5
D10
Vehicle YKL20 CL
Vehicle YKL10 YKL20
B
Ucp1
Pgc1a
Dio2
p=0.22
p=0.06
Veh Y5 Y10 Y20 CL
C
Vehicle
YKL10
YKL20
iWAT
- UCP1
- β-Actin
UCP1 (A.U.)
p=0.26
Veh Y10 Y20
D
Vehicle
YKL10
YKL20
CL
iWAT

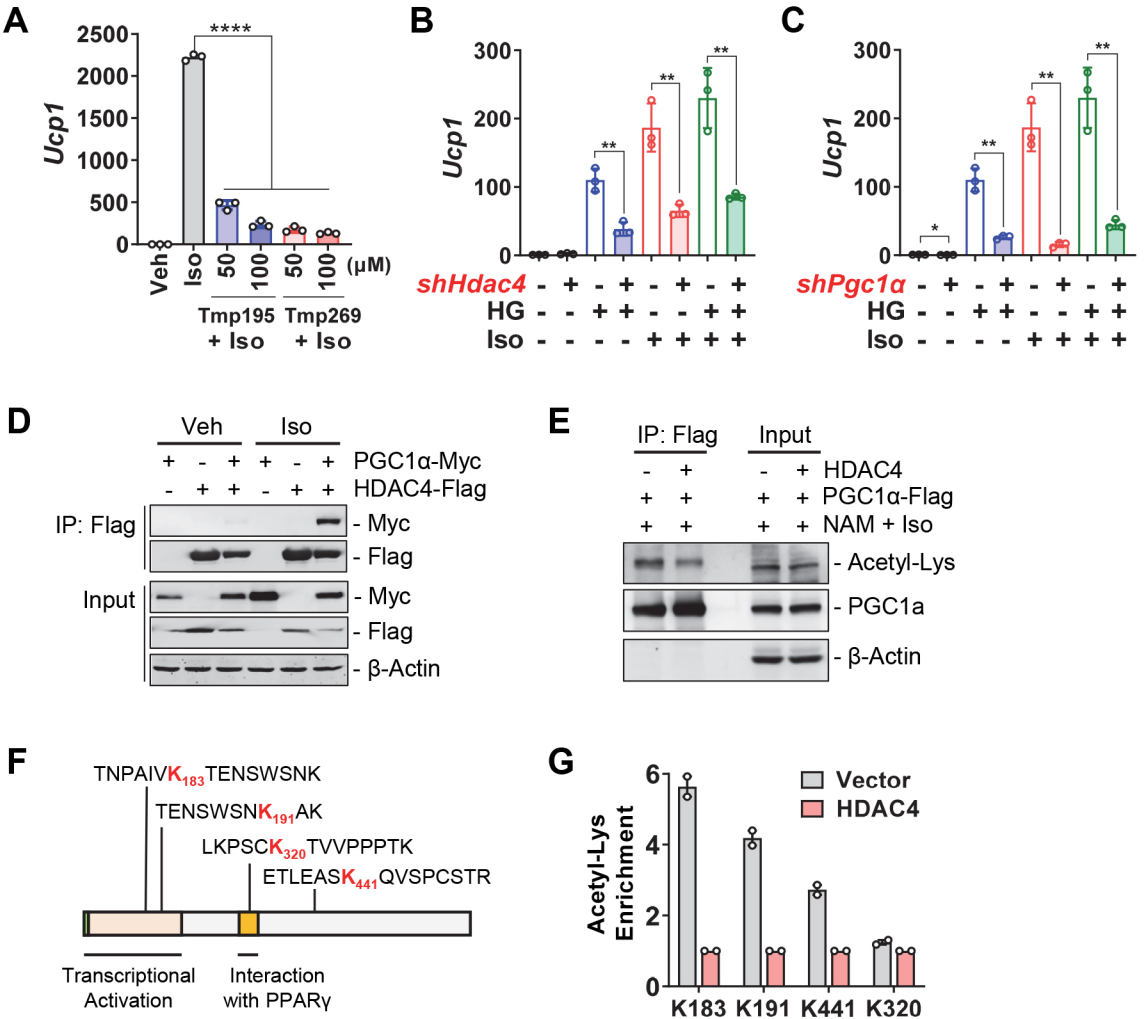
A
Ucp1
2500
2000
1500
1000
500
0
****
Veh
Iso
50
100
50
100
(μM)
Tmp195 + Iso
Tmp269 + Iso
B
Ucp1
300
200
100
0
**
shHdac4
HG
Iso
C
Ucp1
300
200
100
0
*
**
shPgc1α
HG
Iso
D
Veh
Iso
PGC1α-Myc
HDAC4-Flag
IP: Flag
Input
- Myc
- Flag
- β-Actin
E
IP: Flag
Input
HDAC4
PGC1α-Flag
NAM + Iso
- Acetyl-Lys
- PGC1a
- β-Actin
F
TNPAIVK183TENSWSNK
TENSWSNK191AK
LKPSCK320TVVPPPTK
ETLEASK441QVSPCSTR
Transcriptional Activation
Interaction with PPARγ
G
Acetyl-Lys Enrichment
6
4
2
0
Vector
HDAC4
K183
K191
K441
K320